Title

Improved multiparametric MRI discrimination between low-risk prostate cancer and benign tissues in a small cohort of 5α-reductase inhibitor treated individuals as compared with an untreated cohort

Journal

NMR in Biomedicine, 30(5)

ISSN

0952-3480

Authors

Starobinets, Olga
Kurhanewicz, John
Noworolski, Susan M

Publication Date

2017-05-01

DOI

10.1002/nbm.3696

Peer reviewed

HHS Public Access

Author manuscript

NMR Biomed. Author manuscript; available in PMC 2018 May 01.

Published in final edited form as:

NMR Biomed. 2017 May ; 30(5): . doi:10.1002/nbm.3696.

Improved Multiparametric MRI Discrimination Between Low-Risk Prostate Cancer and Benign Tissues in a Small Cohort of 5-alpha Reductase Inhibitor Treated Individuals as Compared to an Untreated Cohort

Olga Starobinets, MS[1,2], **John Kurhanewicz, PhD**[1,2], and **Susan M Noworolski, PhD**[1,2]

[1]Graduate Group in Bioengineering, UCSF and UC Berkeley

[2]Department of Radiology and Biomedical Imaging, UCSF

Abstract

The study purpose was to determine whether 5α-reductase inhibitors (5-ARIs) affect the discrimination between low-grade prostate cancer (PCa) and benign tissues on mpMRI. Twenty men with biopsy-proven Gleason 3+3 PCa and 3T mpMRI were studied. Ten patients (Tx) were receiving 5-ARIs for at least a year at scan time. Ten untreated patients (Un) were matched to the treated cohort. For each subject two regions of interest (ROI) representing cancerous and benign tissues were drawn within the peripheral zone of each prostate, MR measures evaluated, and cancer contrast versus benign [Contrast=(MR_{Tumor}-$MR_{Healthy}$)/$MR_{Healthy}$] calculated. Decreased cancer contrast was noted on T2-weighted images: 0.4 (Un) versus 0.3 (Tx). However, for functional MR measures, a better separation of cancerous and benign tissues was observed in the treated group. Cancer contrast on high-b diffusion weighted images (DWI) was 0.61 (Un) vs. 0.99 (Tx). Logistic regression analysis yielded higher AUC (area under the curve) values for distinguishing cancerous from benign regions in treated subjects on high-b DWI [0.71 (Un), 0.94 (Tx)], maximal enhancement slope [0.95 (Un), 1 (Tx)], peak enhancement [0.84 (Un), 0.93 (Tx)], washout slope [0.78 (Un), 0.99 (Tx)], K^{trans} [0.9 (Un), 1 (Tx)], and combined measures [0.86 (Un), 0.99 (Tx)]. Coefficients of variation for MR measures were lower in benign and cancerous tissues in the treated group compared to the untreated group. This study's results suggest an increase in homogeneity of benign and malignant peripheral zone prostatic tissues with 5-ARI exposure, observed as reduced variability of MR measures after treatment. Cancer discrimination was lower with T2-weighted imaging, but was higher with functional MR measures in a 5-ARI-treated cohort compared to controls.

Keywords

prostate cancer; mpMRI; 5α-reductase inhibitors; finasteride; dutasteride

Corresponding author: Olga Starobinets, Department of Radiology and Biomedical Imaging, UCSF, 185 Berry Street, Suite 350, San Francisco, CA, 94107. Phone: 415-353-4577, Fax: 415-353-9423 , Olga.Starobinets@ucsf.edu.

1. Introduction

One in seven men in the United States will be diagnosed with prostate cancer (PCa) during his lifetime[1]. Currently, prostate cancer is most often detected on systematic ultrasound-guided biopsies prompted by elevated serum prostate specific antigen (PSA) levels. Unfortunately, prostate biopsies are often associated with discomfort, pain, hematuria, rectal bleeding and carry a risk of infection[2]. Additionally, prostate biopsies are inherently limited by sampling errors[3,4]. In recent years, multiparametric magnetic resonance imaging (mpMRI) has emerged as a powerful noninvasive technique for diagnosis, localization, and staging of prostate cancer[5-9]. A growing number of studies attest to the utility of mpMRI in detecting prostate cancer in untreated men[5,6,9] or in identifying recurrent disease in patients treated with definitive therapies (i.e. radiation therapy or radical prostatectomy)[10-14]. However, some men, such as those taking 5α-reductase inhibitors (5-ARI), fall in-between these two categories. Five alpha-reductase inhibitors such as Finasteride or Dutasteride are marketed for management of prostate enlargement known as benign prostatic hyperplasia (BPH), a condition that often contributes to the development of lower urinary tract symptoms in older men. BPH is extremely common. It affects 50% of men by the age of 50 and 90% of men in their 80s[15]. Fifty percent of men in their 60s experience low urinary tract symptoms due to BPH[16]. With growing numbers of men receiving mpMRI scans as part of the active surveillance protocol and with BPH being such a prevalent condition in older men, it is important to evaluate how the 5-ARIs affect the MR imaging and the interpretation of the imaging findings.

The health of the prostate is largely dependent on properly regulated actions of androgens through the androgen receptor (AR) complex[17]. Deregulation of the androgen–androgen receptor pathway plays an important role in the development and progression of prostate cancer[18]. The 5α-reductase enzymes convert testosterone, the most abundant circulating androgen, to dihydrotestosterone (DHT). Increased activity of 5α-reductase results in increased production of DHT. DHT has a greater affinity for the androgen receptor than testosterone and is a more effective activator of the AR. Once activated, the AR sets off a cascade of events resulting in increased cell growth and proliferation characteristic to both BPH and prostate cancer. One approach in regulating the AR pathway is to block the synthesis of DHT and by decreasing the levels of circulating androgens, limit the rates of AR activation and moderate cellular proliferation[19].

MpMRI exams probe the prostate gland on a tissue level; diffusion weighted imaging is used to evaluate cell proliferation, while dynamic contrast enhanced imaging is used to assess neovascularity and tissue structure of the prostate. Since 5-ARIs impact prostatic tissues, the use of 5-ARI agents is expected to affect the interpretation of imaging studies in 5-ARI treated patients. In order to accurately stage and assess disease progression in 5-ARI treated patients, the effects of these agents on imaging studies in both benign and malignant prostatic tissues need to be investigated. The purpose of this study was to determine whether 5-ARIs affect discrimination between low-grade prostate cancer and benign tissues on multiparametric MR imaging.

2. Materials and Methods

2.1. Patients

This study was approved by the Committee on Human Research at this institution and was compliant with the Health Insurance Portability and Accountability Act. Written, informed consent was obtained from all subjects. Twenty patients with biopsy-proven Gleason Score 3+3 (GS3+3) prostate cancer were studied. Ten patients were taking 5-ARIs for at least a year at the time of the study. The ten 5-ARI treated patients were selected from 17 men who were scanned at our institution within the last 2 years, had complete mpMRI studies, were injected with gadopentetate dimeglumine (Gd-DTPA) contrast agent during DCE studies, had GS3+3 disease on biopsy and were taking either Dutasteride or Finasteride for at least a year. Out of these 17 patients, 1 patient was excluded due to a prior cryosurgery and another patient was excluded due to a prior androgen deprivation hormonal therapy. Out of the remaining 15 men, 10 men had mpMRI visible cancers within the peripheral zone of the prostate as per their radiology report and were included in the study. Four out of ten men in the 5-ARI treated group were taking Dutasteride (0.5mg taken daily), while the remaining six were being treated with Finasteride (5mg taken daily). Ten untreated individuals with GS3+3 biopsy-proven peripheral zone cancers, scanned within the same 2-year period as the treated group, with complete mpMRI studies, Gd-DPTA injections during DCE, and with prostate volumes matched to the individuals in the 5-ARI treated group, were identified in the database and included in the study to serve as controls. Prostate volumes were matched to allow for similar central gland/peripheral zone ratios to facilitate comparable cancer detection. Cancer detection can be more challenging in patients with a significantly compressed peripheral zone due to an enlarged central grand. Prostate volumes were matched within 5cc as estimated on the MRI, except for the largest and the smallest prostates that were matched within 8.3cc and 5.5cc respectively. Despite the prostate volume matching, there are likely differences in the peripheral zone and the central gland volumes between the two groups.

Age, PSA values, the number of previous biopsy procedures, the number of biopsy cores obtained during the most recent biopsy procedure, and the number of days between the most recent biopsy and the MR exam, prostate volume, and benign and cancerous regions of interest (ROI) areas were compared between the two groups. The reported PSA values were obtained within a six-month window of the MRI scan.

2.2. MR Imaging

All patients were imaged with an expandable balloon endorectal coil (Medrad, Bayer HealthCare LLC, Whippany, NJ, USA) and a GE phased array on a 3T MR scanner (GE Healthcare, Waukesha, WI, USA). The balloon coil was inflated with a perfluorocarbon fluid (Galden, Solvay Plastics, West Deptford, NJ, USA). T1-weighted images were examined as part of the clinical radiology review to ensure the biopsy hemorrhage was not corrupting the interpretation of the imaging study. T2-weighted images, diffusion-weighted images (DWI), and dynamic contrast-enhanced (DCE) MRI were acquired. The DCE MRI was performed using a single-dose of Gd-DPTA (Magnevist; Bayer HealthCare LLC, Whippany, NJ, USA) over ~5 minutes. Diffusion weighted imaging (DWI) was acquired

using a 2D single-shot spin echo sequence with pixel bandwidth = 1952 (conventional acquisition, n=4: 2 (untreated) and 2 (5-ARI treated)), or pixel bandwidth = 1305 (reduced-field-of-view acquisition[20], n=16: 8 (untreated) and 8 (5-ARI treated)), with b=0 and 600 s/mm^2, as well as b=0 and b=1350 s/mm^2 over 6 non-coplanar, non-colinear directions. The acquisition parameters are outlined in Table 1. T2-weighted and diffusion-weighted images were corrected for the reception profile of the endorectal and the pelvic phased-array coils using Prostate Analytical Coil Correction (PACC) software available on the GE scanners. This correction technique as described in the literature[21,22] has been adopted by GE. High quality of the intensity correction was visually confirmed. Apparent diffusion coefficient (ADC) maps were generated for DW b=0, 600 s/mm^2 images. In-house software was used to create the ADC maps. The maps were computed from the combined DWI (b=600 s/mm^2) and T2-weighted reference images (b=0 s/mm^2) using Equation 1, where b is the b-value used for the diffusion-weighted acquisition, S_{gm} is the geometric mean of the signal intensities acquired over the six gradient directions, and S_0 is the signal intensity of the T2-weighted image acquired without applying diffusion gradients.

$$\mathrm{ADC} = -\frac{1}{\mathrm{b}}\ln\left(\frac{s_{gm}}{s_0}\right) \quad [1]$$

For b=0, 1350 s/mm^2 acquisition, diffusion-weighted images were corrected for the reception profile of the endorectal coil and a mean of the 6 directions was computed to create a high-b value DW image. For completeness, high-b ADC maps were computed for DWI b=0, 1350 s/mm^2 images using Equation 1 and following the same procedure outlined above.

DCE maps were created based on the semi-quantitative tissue enhancement parameters of maximal enhancement slope, peak enhancement, and washout rate[23]. Additionally, pharmacokinetic modeling was performed using the mean signal intensity measurements within individual ROIs. Quantitative DCE parameters of the fractional extravascular, extracellular volume (v_{EES}), the transfer constant (K^{trans}), and the rate constant (K_{ep}) were computed. A widely used two-compartmental extended Tofts-Kermode model was applied since prostate tissue has relatively low permeability and this model is permeability, surface area-limited rather than flow-limited[24]. The concentration of Gd-DTPA in the blood plasma was modeled as a biexponential (Equation 2)[25]

$$\mathrm{C_p} = \mathrm{AmpD}(\mathrm{a_1 e^{-m_1 t}} + \mathrm{a_2 e^{-m_2 t}}) \quad [2]$$

where Amp=5.2, D = 0.1mmol/Kg of Gd-DTPA, a_1 = 3.99 kg/L, m_1 = 0.144 1/min, a_2 = 4.78 kg/L, m_2 = 0.011 1/min. A blood plasma fractional volume of 0.01 was used. The Amp was introduced to account for interpatient differences and was determined by minimizing the root-mean-square error (RMSE) of the fits.

For each subject, a single cancer ROI and a single benign ROI were drawn freeform within the peripheral zone of each prostate on T2-weighted images, following areas of mpMRI concordance. Lesion placement was based upon agreement of biopsy and imaging findings. Benign ROIs were drawn contralateral to each cancerous region with care taken to avoid areas with positive biopsy findings. Additionally, locations for biopsy cores containing HGPIN or prostatitis were noted and avoided when placing benign regions of interest. All ROIs were drawn in the PZ. The ROIs were drawn without knowledge of the patients' treatment status. T2-weighted image intensity, ADC, high-b value DWI intensity, high-b ADC, maximal enhancement slope, peak enhancement, washout slope, v_{EES}, K^{trans}, and K_{ep} values were computed for each region of interest.

T2-weighted images and high-b value diffusion-weighted images are not measured on an absolute scale. For these measures, changes in gain may contribute additional variability across subjects. To account for this, contrast values between the cancerous and benign tissues were calculated based on Equation 3.

$$\text{Contrast} = \frac{\text{MR}_{\text{Tumor}} - \text{MR}_{\text{Healthy}}}{\text{MR}_{\text{Healthy}}} \quad [3]$$

Where “MR” represents the MR measure of interest, i.e. T2-weighted or high-b value DWI intensity.

2.3. Statistical Methods

Statistical analyses were carried out using JMP software (JMP, Version 12, SAS Institute Inc., Cary, NC). Measures are reported as mean ± standard deviation, with median (first quartile, third quartile), as well as minimum and maximum values also reported. Two-tailed, heteroscedastic Student's t-tests were used to compare age, PSA, prostate volume, as well as the sizes of benign and cancerous ROIs between the two groups, with $p \leq 0.05$ considered statistically significant. The number of biopsy procedures, the number of biopsy cores obtained during the most recent biopsy, and the number of days since the most recent biopsy procedure were compared between the two groups using Mann-Whitney rank-sum test. Two-tailed, heteroscedastic Student's t-tests with a significance level of 0.05 were also used to compare MR measures in the untreated and the 5-ARI treated groups. Ordinal logistic regression analysis was performed for all imaging modalities to evaluate the area under the ROC (receiver operating characteristic) curve (AUC) in benign and cancerous regions for the untreated and the 5-ARI treated groups. A forward stepwise logistic regression with a threshold p-value of 0.1 was used to identify the imaging parameters for inclusion in the combined model. Finally, the coefficient of variation (COV) was evaluated for all imaging modalities for benign and cancerous regions in both the untreated and the 5-ARI treated groups.

3. Results

Patient characteristics for the untreated and the 5-ARI treated patients are summarized in Table 2. No significant differences were noted between the two groups. The untreated and the 5-ARI treated groups were similar in age (p=0.1), PSA (p=0.77), the number of previous biopsy procedures (p=0.81), the number of biopsy cores obtained during the most recent biopsy (p=0.85) and prostate volumes (p=0.90). Additionally, none of the subjects included in the analysis were noted to have post biopsy hemorrhage evident on imaging. The number of days between the most recent biopsy procedure and the MR exam was fewer in the untreated group than the 5-ARI treated group (Table 2); however, the difference between the two groups was not statistically significant p=0.27.

No statistically significant differences were noted between the sizes of the benign ROI areas for the untreated and the 5-ARI treated groups (p=0.24). Additionally, no statistically significant differences were noted between the sizes of the malignant ROI areas for the untreated and the 5-ARI treated groups (p=0.58). The two groups also had similar incidence of biopsy detected HGPIN and prostatitis. One patient in each group had a single HGPIN core discovered on biopsy. Additionally one patient in each group had biopsy- diagnosed prostatitis.

No significant differences between the untreated and the 5-ARI treated groups were noted for benign or cancerous regions on T2-weighted imaging, ADC, high-b value DWI intensity, high-b ADC, maximal enhancement slope, peak enhancement, washout slope, or v_{EES}. No significant differences were noted for cancerous tissues between the untreated and the 5-ARI treated groups on K^{trans} and K_{ep} measures. However, significant differences were noted between benign untreated and benign treated tissues on K^{trans} ($p<0.02$) and K_{ep} ($p<0.03$). For benign tissues K^{trans} values were 0.42 ± 0.234 min^{-1} and 0.20 ± 0.09 min^{-1}, while K_{ep} values were 1.86 ± 1.25 min^{-1} and 0.70 ± 0.41 min^{-1} for the untreated and the 5-ARI treated groups respectively.

Example images for a patient with a low-grade biopsy-proven (GS3+3) prostate cancer with a PSA of 4.6 ng/ml are shown in the top row of Figure 1. The patient was not taking any medication for BPH or lower urinary tract symptoms. The bottom row in Figure 1 depicts example images for another patient with a biopsy-proven (GS3+3) prostate cancer with a PSA of 0.42 ng/ml who had been taking Dutasteride for the prior year. Based on visual assessment, Figure 1 demonstrates a better discrimination of benign and malignant tissues on the high-b value intensity images and the washout images in the treated case when compared to the untreated example.

Figure 2 depicts box-plots for the MR measures and calculated maps in benign and cancerous tissues as observed for the untreated men and the individuals treated with 5-ARIs. For ADC, high-b value DWI intensity, high-b ADC, peak enhancement, maximal enhancement slope, washout slope, K^{trans}, and K_{ep} a better separation of benign and cancerous tissues was observed for individuals treated with 5-ARIs than for those untreated.

Table 3 lists ROC AUC values obtained when stepwise logistic regression was performed for all the imaging modalities for untreated and 5-ARI treated subjects in benign and cancerous

regions. The ROC AUC values for distinguishing benign tissues from cancer were consistently higher in the treated group with the exception of T2-weighted images (AUC of 0.82 for the untreated and 0.79 for the 5-ARI treated group) and both sets of ADC images (untreated and 5-ARI treated groups both had an AUC of 1).

In order to account for the arbitrary intensity scales associated with T2w and high-b DWI, tumor contrast was evaluated. For the T2w, tumor contrast was computed to be 0.40±0.13 and 0.30±0.20 for the untreated and the 5-ARI treated groups, respectively, p=0.19. For high-b DWI intensity measures, contrast values were 0.61±0.43 and 0.99±0.52 for the untreated and the 5-ARI treated groups respectively, p=0.086.

The absolute coefficients of variation for the measures within the benign tissues and within the cancer are listed in Table 4. COV values were lower in both the benign tissues and the cancer for the treated group compared to the untreated group for high-b value DW images, high-b ADC, peak enhancement, washout slope, v_{EES}, K_{ep}, and maximal enhancement slope (cancer only), ADC and K^{trans} (benign only).

4. Discussion

Dutasteride and Finasteride are two commonly used drugs prescribed for treatment of prostate enlargement. Both agents act as inhibitors to the 5α-reductase enzyme, forming strong irreversible ternary complexes with the 5α-reductase–NADPH complex[26]. In a 2011, multicenter, randomized, double-blind, 12 month-long study of 1630 men, Nickel *et al.* reported that both Dutasteride and Finasteride were effective at reducing prostate volume with no significant difference between the two treatments during the study and with a similar number of adverse events [27].

This study investigated whether 5-ARIs affect discrimination between low-grade prostate cancer and benign tissues on mpMRI. It was observed that high-b value DWI intensity, maximal enhancement slope, peak enhancement, washout slope, K^{trans}, and K_{ep} acquired as part of a routine prostate mpMRI scan show reduced variability within both low-grade (GS3+3) cancerous tissues and within benign tissues in the treated group. Additionally, a better separation between cancerous and benign regions was noted for the prostate tissues exposed to 5-ARI as compared to the untreated prostate tissues. These results are consistent with the findings of an earlier study that monitored the effects of Dutasteride on untreated prostate cancer using MRI and magnetic resonance spectroscopic imaging (MRSI)[28]. The authors reported that in tumors the levels of the metabolite choline, the presence of which signals malignancy, remained unchanged with 5-ARI treatments. However, in benign prostatic tissues, 5-ARI treatments resulted in decreased levels of the prostatic secretory metabolites citrate and polyamines, low levels of which are consistent with 5-ARIs primarily inhibiting metabolism of healthy prostatic glandular tissues and eventually inducing atrophy of these tissues[28]. The reduction of the dominant normal prostatic metabolite MR resonances increases the visibility of the cancerous metabolite signals, elevated choline to citrate ratio, and therefore the detection of small amounts of cancer[28]. By blocking the AR pathway, 5-ARIs block DHT driven proliferation and vascularization of prostatic tissues, inducing apoptosis and resulting in increased amounts of tissue atrophy. When exposed to 5-

ARI therapy, androgen sensitive glandular normal and BPH tissues quickly atrophy, while less androgen sensitive cancers will atrophy more slowly[29]. Based upon this biology and our results, we suggest that 5-ARI therapy results in decreased contribution of glandular tissues to all MR measurements and allows cancerous tissues to become readily apparent against a more uniform background of atrophic tissues.

Untreated benign and 5-ARI treated benign prostatic tissues have different appearances on histopathological examination. Histologically, atrophy is characterized by a reduction in the volume of existing glands and the loss of luminal secretary epithelial cells[30]. Large pools of lumen are observed for healthy untreated prostatic tissues, while significantly diminished luminal spaces and increased surfaces of stromal tissues are typically seen in the treated individuals. Additionally, the shrinking and loss of the basal and the secretory epithelial cells associated with atrophy is often noted in the treated prostatic tissues.

Figure 3 shows an example of T2-weighted images for benign tissues for two untreated and one 5-ARI treated patients. Figure 3A demonstrates the appearance of healthy glandular tissues in an untreated patient; detecting cancerous lesions against such a uniform and bright background is straightforward. Unfortunately, very few prostates have such an uncomplicated, glandular appearance. Figure 3B demonstrates the challenges associated with detecting cancers within mixed tissues, characteristic of the majority of prostates. Against a background of such heterogeneous tissues – some glandular and bright, some stromal and dark, some atrophic, some inflamed, and some malignant - it is much more challenging to confidently identify cancerous regions in this untreated patient. Figure 3C shows why atrophic processes associated with 5-ARI treatments may enhance the diagnostic utility of mpMRI. While the 5-ARI treated prostatic tissues of the peripheral zone appear darker than those observed in healthy, untreated tissues (Figure 3A), the diffuse nature of the hormone-induced atrophy allows for a more uniform background than the mix of tissues often seen in untreated prostates (Figure 3B). The uniformity of the benign prostatic tissues provides a better background against which a malignant lesion can be detected. This may explain why we observe a better separation between benign and malignant tissues and a lower variability in the measures for 5-ARI treated group when compared to untreated controls.

Within the scope of anti-androgen therapies, very few studies review the effects of 5-ARI agents on imaging[28]. For instance, Dutasteride treatment was shown to increase the rate of cancer detection in ultrasound studies[31-33]. However, in the realm of MR imaging, most of the published literature involving 5-ARI agents focuses on the changes in prostate volumes due to androgen deprivation[34,35]. There are, however, studies covering the effects of hormone ablation on both anatomical and functional prostate MR imaging[36-41]. There is a consensus that glandular atrophy and tissue shrinkage makes prostate cancer detection more challenging on T2-weighted images[40-42]. This is a similar observation to what is seen for T2-weighted images in the 5-ARI treated cases of the current study. For functional imaging, preliminary studies have shown cancerous lesions becoming less apparent on DWI and DCE post-hormonal ablation, which is different than the results of the current study[36,39]. This discrepancy is likely due to the differences in the evaluated populations. Hormonal ablation is typically used to treat aggressive prostate cancer rather than GS3+3 disease (pooling the

patients from the two ablation studies - only 4/69 men had GS3+3 prostate cancers[36,39]), which is vastly different from our exclusively low-risk GS3+3 cohort. Pretreatment discrimination of cancer and benign tissues is easier in patients with aggressive prostate cancer as opposed to those with low-risk disease. Thus, inhomogeneity of prostatic tissues plays a small role in identifying aggressive, clear-cut cancers, but is a significant hurdle in diagnosing diffuse or low-grade lesions. For low-risk cancers, as our data suggests, post-treatment cancer detection might be advantaged by the atrophy of benign tissues, especially when considering the challenges of low-risk cancer detection pre-treatment. On the other hand, atrophy of benign glandular tissues post-treatment might make it more challenging to detect aggressive cancers when compared to the ease of detection pre-treatment as suggested by the prior studies of hormone ablation in aggressive cancer[36,39].

In the current study, while it was noted that the contrast on T2-weighted images between cancerous and benign tissues was lower in the 5-ARI treated than the untreated group, our findings for the functional imaging measures provide reassurance. First, contrast on the high-b value DW images between cancerous and malignant tissues was higher in the 5-ARI treated than the untreated group. Second, the separation between imaging values for cancerous and benign regions was greater on ADC, high-b value DW, maximal enhancement slope, peak enhancement, washout slope, K^{trans}, and K_{ep} images, with an overall reduced variability in the MR measures for individuals in the 5-ARI group. Third, K_{ep} and K^{trans} values obtained for benign regions were significantly lower for the 5-ARI treated than the untreated groups. Higher K_{ep} and K^{trans} values typically signal higher perfusion and are often indicative of malignancy. Since there were no significant differences between K_{ep} and K^{trans} values for the cancerous 5-ARI treated and untreated groups, the larger separation between cancerous and benign tissues in the treated group may potentially lead to an easier detection of cancerous regions in that cohort.

For patients on active surveillance with emphasis placed on detecting and treating more aggressive disease, why do we care about detecting GS3+3 lesions? Several studies reported that patients with visible lesions on mpMRI have an increased overall risk of cancer progression[43,44]; therefore, identifying these lesions is of clinical importance. If pretreatment with 5-ARI agents makes lesions more conspicuous on imaging, it may aid in identifying patients at a higher risk of cancer progression, prompting a closer observation of these patients while on active surveillance. Additionally, while our study looked at GS3+3 disease in 5-ARI treated and untreated men, we expect our findings to be applicable in detection of higher-grade cancer (i.e. GS3+4 or GS4+3 disease), the detection of which is of clinical significance. In this study, we limited the inclusion criteria to GS3+3 lesions in order to avoid introducing variability associated with Gleason 4 disease, especially when detected on biopsy; however, we expect the underlying principle of elucidating cancer against a more homogeneous atrophic background to be applicable for higher grade cancers. This observation that pretreatment with 5-ARI agents improves PCa detection on mpMRI is very similar to the reported effects of 5-ARI agents on the sensitivity of PSA in detecting prostate cancer in 5-ARI treated individuals. In a large study of 18,882 men, Thompson *et al* reported that PSA had a better sensitivity for detecting all grades of prostate cancer in the group treated with Finasteride when compared to a placebo cohort[45]. This further supports the idea

that reducing the impact of potential confounders such as benign pathologies improves cancer detection in the prostate.

Another potentially important consequence of our findings pertains to interpretation of mpMR imaging studies acquired in 5-ARI treated patients when using Prostate Imaging – Reporting and Data System (PI-RADS) criteria. For peripheral zone lesions, PI-RADS places a particular importance on conspicuity of prostatic lesions on diffusion-weighted imaging[46]. Our results suggest that 5-ARI treated patients will have prostate cancers that are more conspicuous on functional imaging than lesions of similar grade in the untreated group. This can potentially lead to a misdiagnosis of higher-grade cancer in men with GS3+3 disease, affecting the disease management for those patients. Knowledge of a patient's 5-ARI status prior to interpretation of his imaging study might be an important caveat when applying PI-RADS criteria.

Our study had several limitations. First, with only 10 patients per group our study has a small sample size. Second, biopsy-based Gleason grading of cancerous regions was used, which could be inaccurate due to biopsy sampling errors[3,4]. Third, only men with visible lesions on mpMRI were included in our study, which introduces a selection bias to our sample. However, this selection bias adds clinical significance to our findings. Men with lesions visible on mpMRI have been shown to have an increased risk of cancer progression; therefore, detecting these lesions in 5-ARI treated individuals is important for disease management in this population. Fourth, benign regions were drawn based on imaging (contralateral to cancer); they could potentially include inflammation or even cancer undetected on biopsy. Fifth, T2w measures were reported for completeness; however, these measures are inherently biased since the ROIs were drawn on T2w images, with the size of the lesion providing further bias. Additionally, while untreated patients were matched to the treated individuals and were not significantly different in the demographic, clinical, and biopsy metrics tested, there could be unaccounted for differences between the two subject groups. For purposes of completeness we are reporting both semi-quantitative parameters, as well as measures derived using quantitative pharmacokinetic modeling. It is important to remember that these measures are not independent but may be attributed to similar biological mechanisms. Similarly, there is a redundancy to ADC (b=600 s/mm^2) and high-b ADC (b=1350 s/mm^2) maps, with the two sets of data representing the same biological processes but at slightly different levels of tissue organization. Finally, patients were treated with either Finasteride (type I 5-ARI) or Dutasteride (type I and II 5-ARI). Differences between the two agents may introduce variability to the data. However, despite these limitations, for the majority of the imaging modalities, we were still able to see reduced coefficients of variation and better discrimination between cancerous and benign tissues in the treated patients as compared to the untreated patients.

5. Conclusion

This study presented data from 5-ARI treated and untreated men receiving 3T multiparametric MRI scans. A better separation between low-grade cancerous and benign regions was observed for prostatic tissues exposed to 5-ARIs for the majority of the MR measures of interest and overall with an mpMRI approach. Furthermore, a reduction in the

coefficient of variation was noted for most of the MR measures in the treated cohort (for both cancerous and benign regions) when compared to the untreated group. The findings in our study suggest that pretreatment with 5-ARI may facilitate a better discrimination of low-grade prostate cancer from benign tissues with mpMRI. Furthermore, this study suggests that interpretation of mpMRI in treated patients may need to be refined, as both more high-risk lesions may be identified and as low-risk lesions may be misdiagnosed as more aggressive. These findings are of clinical importance and require further exploration in a larger cohort.

Acknowledgments

Grant Support: NIH R01 CA148708, NIH R01 CA137207

References

1. Siegel RL, Miller KD, Jemal A. Cancer Statistics, 2016. Ca-Cancer J Clin. 2016; 66(1):7–30. [PubMed: 26742998]
2. Loeb S, Vellekoop A, Ahmed HU, Catto J, Emberton M, Nam R, Rosario DJ, Scattoni V, Lotan Y. Systematic review of complications of prostate biopsy. European urology. 2013; 64(6):876–892. [PubMed: 23787356]
3. Fernandes ET, Sundaram CP, Long R, Soltani M, Ercole CJ. Biopsy Gleason score: how does it correlate with the final pathological diagnosis in prostate cancer? British journal of urology. 1997; 79(4):615–617. [PubMed: 9126095]
4. Steinberg DM, Sauvageot J, Piantadosi S, Epstein JI. Correlation of prostate needle biopsy and radical prostatectomy Gleason grade in academic and community settings. The American journal of surgical pathology. 1997; 21(5):566–576. [PubMed: 9158682]
5. de Rooij M, Hamoen EH, Futterer JJ, Barentsz JO, Rovers MM. Accuracy of multiparametric MRI for prostate cancer detection: a meta-analysis. AJR American journal of roentgenology. 2014; 202(2):343–351. [PubMed: 24450675]
6. Hegde JV, Mulkern RV, Panych LP, Fennessy FM, Fedorov A, Maier SE, Tempany CM. Multiparametric MRI of prostate cancer: an update on state-of-the-art techniques and their performance in detecting and localizing prostate cancer. Journal of magnetic resonance imaging : JMRI. 2013; 37(5):1035–1054. [PubMed: 23606141]
7. Hoeks CM, Barentsz JO, Hambrock T, Yakar D, Somford DM, Heijmink SW, Scheenen TW, Vos PC, Huisman H, van Oort IM, Witjes JA, Heerschap A, Futterer JJ. Prostate cancer: multiparametric MR imaging for detection, localization, and staging. Radiology. 2011; 261(1):46–66. [PubMed: 21931141]
8. Isebaert S, Van den Bergh L, Haustermans K, Joniau S, Lerut E, De Wever L, De Keyzer F, Budiharto T, Slagmolen P, Van Poppel H, Oyen R. Multiparametric MRI for prostate cancer localization in correlation to whole-mount histopathology. Journal of magnetic resonance imaging : JMRI. 2013; 37(6):1392–1401. [PubMed: 23172614]
9. Turkbey B, Pinto PA, Mani H, Bernardo M, Pang Y, McKinney YL, Khurana K, Ravizzini GC, Albert PS, Merino MJ, Choyke PL. Prostate cancer: value of multiparametric MR imaging at 3 T for detection--histopathologic correlation. Radiology. 2010; 255(1):89–99. [PubMed: 20308447]
10. Arumainayagam N, Kumaar S, Ahmed HU, Moore CM, Payne H, Freeman A, Allen C, Kirkham A, Emberton M. Accuracy of multiparametric magnetic resonance imaging in detecting recurrent prostate cancer after radiotherapy. BJU international. 2010; 106(7):991–997. [PubMed: 20230392]
11. Barchetti F, Panebianco V. Multiparametric MRI for recurrent prostate cancer post radical prostatectomy and postradiation therapy. BioMed research international. 2014; 2014:316272. [PubMed: 24967355]
12. Tamada T, Sone T, Jo Y, Hiratsuka J, Higaki A, Higashi H, Ito K. Locally recurrent prostate cancer after high-dose-rate brachytherapy: the value of diffusion-weighted imaging, dynamic contrast-

enhanced MRI, and T2-weighted imaging in localizing tumors. AJR American journal of roentgenology. 2011; 197(2):408–414. [PubMed: 21785087]

13. Vargas HA, Wassberg C, Akin O, Hricak H. MR imaging of treated prostate cancer. Radiology. 2012; 262(1):26–42. [PubMed: 22190655]
14. Westphalen AC, Reed GD, Vinh PP, Sotto C, Vigneron DB, Kurhanewicz J. Multiparametric 3T endorectal mri after external beam radiation therapy for prostate cancer. Journal of magnetic resonance imaging : JMRI. 2012; 36(2):430–437. [PubMed: 22535708]
15. Roehrborn CG. Benign prostatic hyperplasia: an overview. Reviews in urology. 2005; 7(Suppl 9):S3–S14.
16. Chute CG, Panser LA, Girman CJ, Oesterling JE, Guess HA, Jacobsen SJ, Lieber MM. The prevalence of prostatism: a population-based survey of urinary symptoms. The Journal of urology. 1993; 150(1):85–89. [PubMed: 7685427]
17. Heinlein CA, Chang C. Androgen receptor in prostate cancer. Endocrine reviews. 2004; 25(2):276–308. [PubMed: 15082523]
18. Knudsen KE, Penning TM. Partners in crime: deregulation of AR activity and androgen synthesis in prostate cancer. Trends in endocrinology and metabolism: TEM. 2010; 21(5):315–324. [PubMed: 20138542]
19. Nacusi LP, Tindall DJ. Targeting 5alpha-reductase for prostate cancer prevention and treatment. Nature reviews Urology. 2011; 8(7):378–384. [PubMed: 21629218]
20. Korn N, Kurhanewicz J, Banerjee S, Starobinets O, Saritas E, Noworolski S. Reduced-FOV excitation decreases susceptibility artifact in diffusion-weighted MRI with endorectal coil for prostate cancer detection. Magnetic resonance imaging. 2015; 33(1):56–62. [PubMed: 25200645]
21. Moyher SE, Vigneron DB, Nelson SJ. Surface Coil Mr-Imaging of the Human Brain with an Analytic Reception Profile Correction. Jmri-J Magn Reson Im. 1995; 5(2):139–144.
22. Noworolski SM, Reed GD, Kurhanewicz J, Vigneron DB. Post-processing correction of the endorectal coil reception effects in MR spectroscopic imaging of the prostate. Journal of magnetic resonance imaging : JMRI. 2010; 32(3):654–662. [PubMed: 20815064]
23. Noworolski SM, Henry RG, Vigneron DB, Kurhanewicz J. Dynamic contrast-enhanced MRI in normal and abnormal prostate tissues as defined by biopsy, MRI, and 3D MRSI. Magnetic resonance in medicine. 2005; 53(2):249–255. [PubMed: 15678552]
24. Tofts PS, Brix G, Buckley DL, Evelhoch JL, Henderson E, Knopp MV, Larsson HB, Lee TY, Mayr NA, Parker GJ, Port RE, Taylor J, Weisskoff RM. Estimating kinetic parameters from dynamic contrast-enhanced T(1)-weighted MRI of a diffusable tracer: standardized quantities and symbols. Journal of magnetic resonance imaging : JMRI. 1999; 10(3):223–232. [PubMed: 10508281]
25. Tofts PS, Kermode AG. Measurement of the blood-brain barrier permeability and leakage space using dynamic MR imaging. 1. Fundamental concepts. Magnetic resonance in medicine. 1991; 17(2):357–367. [PubMed: 2062210]
26. Aggarwal S, Thareja S, Verma A, Bhardwaj TR, Kumar M. An overview on 5alpha-reductase inhibitors. Steroids. 2010; 75(2):109–153. [PubMed: 19879888]
27. Nickel JC, Gilling P, Tammela TL, Morrill B, Wilson TH, Rittmaster RS. Comparison of dutasteride and finasteride for treating benign prostatic hyperplasia: the Enlarged Prostate International Comparator Study (EPICS). BJU international. 2011; 108(3):388–394. [PubMed: 21631695]
28. Chung HT, Noworolski SM, Kurhanewicz J, Weinberg V, Roach Iii M. A pilot study of endorectal magnetic resonance imaging and magnetic resonance spectroscopic imaging changes with dutasteride in patients with low risk prostate cancer. BJU international. 2011; 108(8 Pt 2):E164–170. [PubMed: 21435153]
29. Rittmaster RS, Norman RW, Thomas LN, Rowden G. Evidence for atrophy and apoptosis in the prostates of men given finasteride. The Journal of clinical endocrinology and metabolism. 1996; 81(2):814–819. [PubMed: 8636309]
30. Wang X, Kruithof-de Julio M, Economides KD, Walker D, Yu H, Halili MV, Hu YP, Price SM, Abate-Shen C, Shen MM. A luminal epithelial stem cell that is a cell of origin for prostate cancer. Nature. 2009; 461(7263):495–500. [PubMed: 19741607]

31. Halpern EJ, Gomella LG, Forsberg F, McCue PA, Trabulsi EJ. Contrast enhanced transrectal ultrasound for the detection of prostate cancer: a randomized, double-blind trial of dutasteride pretreatment. The Journal of urology. 2012; 188(5):1739–1745. [PubMed: 22998915]
32. Ives EP, Gomella LG, Halpern EJ. Effect of dutasteride therapy on Doppler US evaluation of prostate: preliminary results. Radiology. 2005; 237(1):197–201. [PubMed: 16183933]
33. Mitterberger M, Pinggera G, Horninger W, Strasser H, Halpern E, Pallwein L, Gradl J, Bartsch G, Frauscher F. Dutasteride prior to contrast-enhanced colour Doppler ultrasound prostate biopsy increases prostate cancer detection. European urology. 2008; 53(1):112–117. [PubMed: 17321668]
34. Truong H, Logan J, Turkbey B, Siddiqui MM, Rais-Bahrami S, Hoang AN, Pusateri C, Shuch B, Walton-Diaz A, Vourganti S, Nix J, Stamatakis L, Harris C, Chua C, Choyke PL, Wood BJ, Pinto PA. MRI characterization of the dynamic effects of 5alpha-reductase inhibitors on prostate zonal volumes. The Canadian journal of urology. 2013; 20(6):7002–7007. [PubMed: 24331340]
35. Robertson NL, Moore CM, Ambler G, Bott SR, Freeman A, Gambarota G, Jameson C, Mitra AV, Whitcher B, Winkler M, Kirkham A, Allen C, Emberton M. MAPPED study design: a 6 month randomised controlled study to evaluate the effect of dutasteride on prostate cancer volume using magnetic resonance imaging. Contemporary clinical trials. 2013; 34(1):80–89. [PubMed: 23085153]
36. Barrett T, Gill AB, Kataoka MY, Priest AN, Joubert I, McLean MA, Graves MJ, Stearn S, Lomas DJ, Griffiths JR, Neal D, Gnanapragasam VJ, Sala E. DCE and DW MRI in monitoring response to androgen deprivation therapy in patients with prostate cancer: a feasibility study. Magnetic resonance in medicine. 2012; 67(3):778–785. [PubMed: 22135228]
37. Groenendaal G, van Vulpen M, Pereboom SR, Poelma-Tap D, Korporaal JG, Monninkhof E, van der Heide UA. The effect of hormonal treatment on conspicuity of prostate cancer: implications for focal boosting radiotherapy. Radiotherapy and oncology : journal of the European Society for Therapeutic Radiology and Oncology. 2012; 103(2):233–238. [PubMed: 22265733]
38. Hotker AM, Mazaheri Y, Zheng J, Moskowitz CS, Berkowitz J, Lantos JE, Pei X, Zelefsky MJ, Hricak H, Akin O. Prostate Cancer: assessing the effects of androgen-deprivation therapy using quantitative diffusion-weighted and dynamic contrast-enhanced MRI. European radiology. 2015; 25(9):2665–2672. [PubMed: 25820537]
39. Kim AY, Kim CK, Park SY, Park BK. Diffusion-weighted imaging to evaluate for changes from androgen deprivation therapy in prostate cancer. AJR American journal of roentgenology. 2014; 203(6):W645–650. [PubMed: 25415730]
40. Padhani AR, MacVicar AD, Gapinski CJ, Dearnaley DP, Parker GJ, Suckling J, Leach MO, Husband JE. Effects of androgen deprivation on prostatic morphology and vascular permeability evaluated with mr imaging. Radiology. 2001; 218(2):365–374. [PubMed: 11161148]
41. Chen M, Hricak H, Kalbhen CL, Kurhanewicz J, Vigneron DB, Weiss JM, Carroll PR. Hormonal ablation of prostatic cancer: effects on prostate morphology, tumor detection, and staging by endorectal coil MR imaging. AJR American journal of roentgenology. 1996; 166(5):1157–1163. [PubMed: 8615261]
42. Nakashima J, Imai Y, Tachibana M, Baba S, Hiramatsu K, Murai M. Effects of endocrine therapy on the primary lesion in patients with prostate carcinoma as evaluated by endorectal magnetic resonance imaging. Cancer. 1997; 80(2):237–241. [PubMed: 9217036]
43. Fradet V, Kurhanewicz J, Cowan JE, Karl A, Coakley FV, Shinohara K, Carroll PR. Prostate Cancer Managed with Active Surveillance: Role of Anatomic MR Imaging and MR Spectroscopic Imaging. Radiology. 2010; 256(1):176–183. [PubMed: 20505068]
44. Park BH, Jeon HG, Choo SH, Jeong BC, Seo SI, Jeon SS, Choi HY, Lee HM. Role of multiparametric 3.0-Tesla magnetic resonance imaging in patients with prostate cancer eligible for active surveillance. BJU international. 2014; 113(6):864–870. [PubMed: 24053308]
45. Thompson IM, Chi C, Ankerst DP, Goodman PJ, Tangen CM, Lippman SM, Lucia MS, Parnes HL, Coltman CA Jr. Effect of finasteride on the sensitivity of PSA for detecting prostate cancer. Journal of the National Cancer Institute. 2006; 98(16):1128–1133. [PubMed: 16912265]
46. Weinreb JC, Barentsz JO, Choyke PL, Cornud F, Haider MA, Macura KJ, Margolis D, Schnall MD, Shtern F, Tempany CM, Thoeny HC, Verma S. PI-RADS Prostate Imaging - Reporting and Data System: 2015, Version 2. European urology. 2016; 69(1):16–40. [PubMed: 26427566]

Abbreviations

5-ARIs	5α-reductase inhibitors
ADC	apparent diffusion coefficient
AR	androgen receptor
AUC	area under the receiver operating characteristics curve
BPH	benign prostatic hyperplasia
COV	coefficient of variation
DCE	dynamic contrast-enhanced
DHT	dihydrotestosterone
DWI	diffusion weighted imaging
Gd-DTPA	gadopentetate dimeglumine
GS	Gleason Score
$\mathbf{K_{ep}}$	rate constant between extracellular extravascular space and plasma space
$\mathbf{K^{trans}}$	volume transfer constant
MP	multiparametric
MRSI	magnetic resonance spectroscopic imaging
PCa	prostate cancer
PI-RADS	Prostate Imaging – Reporting and Data System
PSA	prostate specific antigen
PZ	peripheral zone
ROI	region of interest
Tx	treated
Un	untreated
$\mathbf{v_{EES}}$	fractional extravascular, extracellular volume

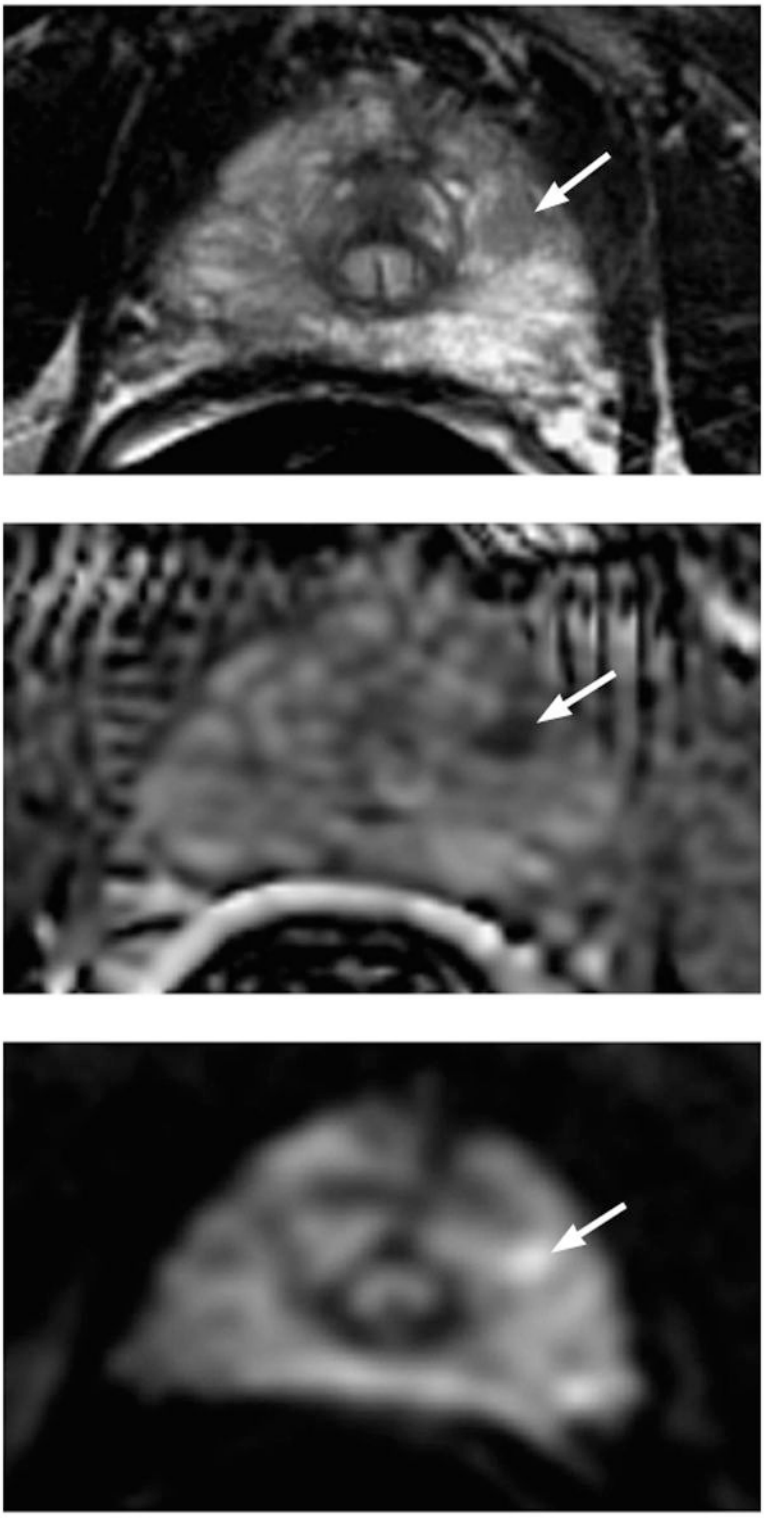

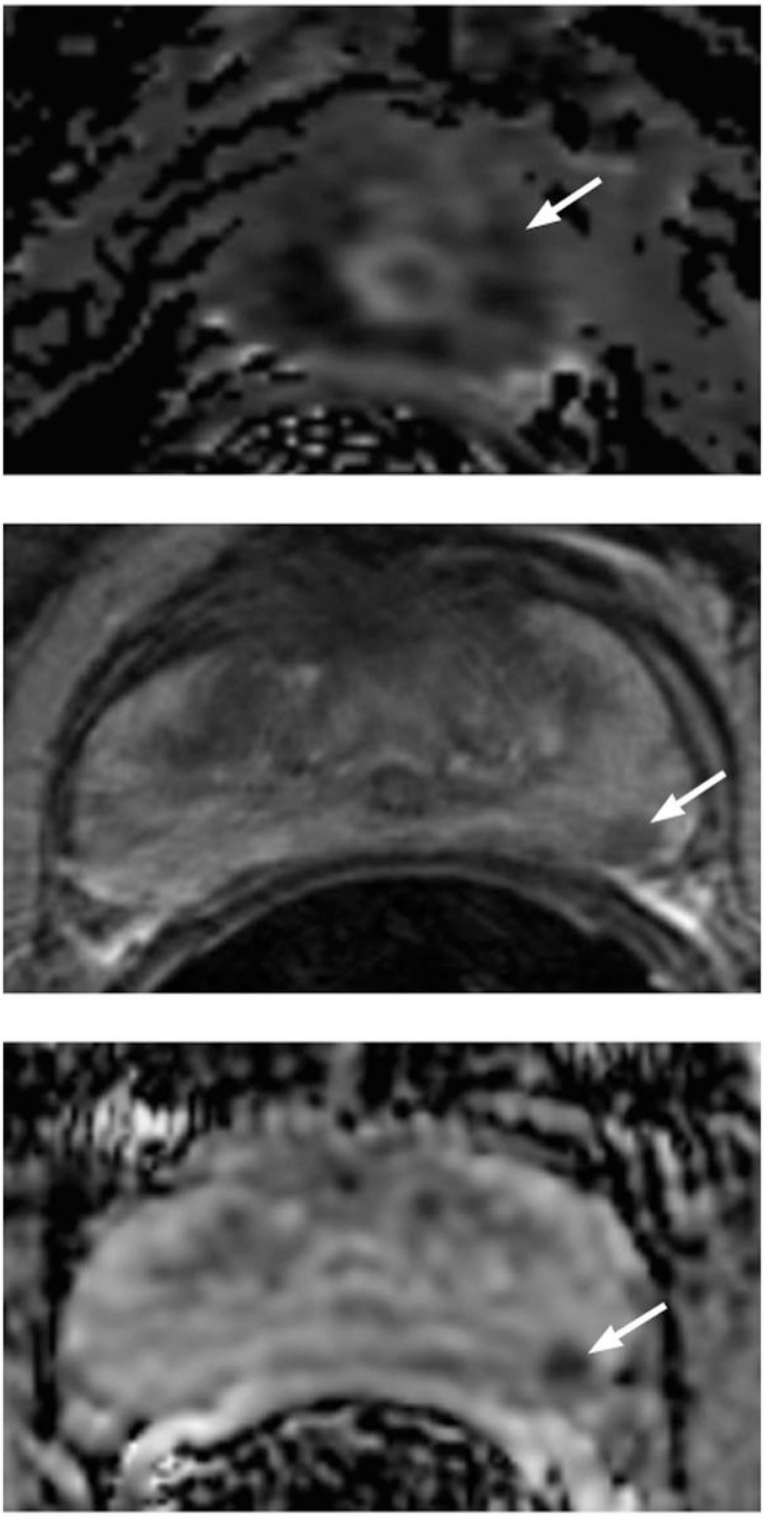

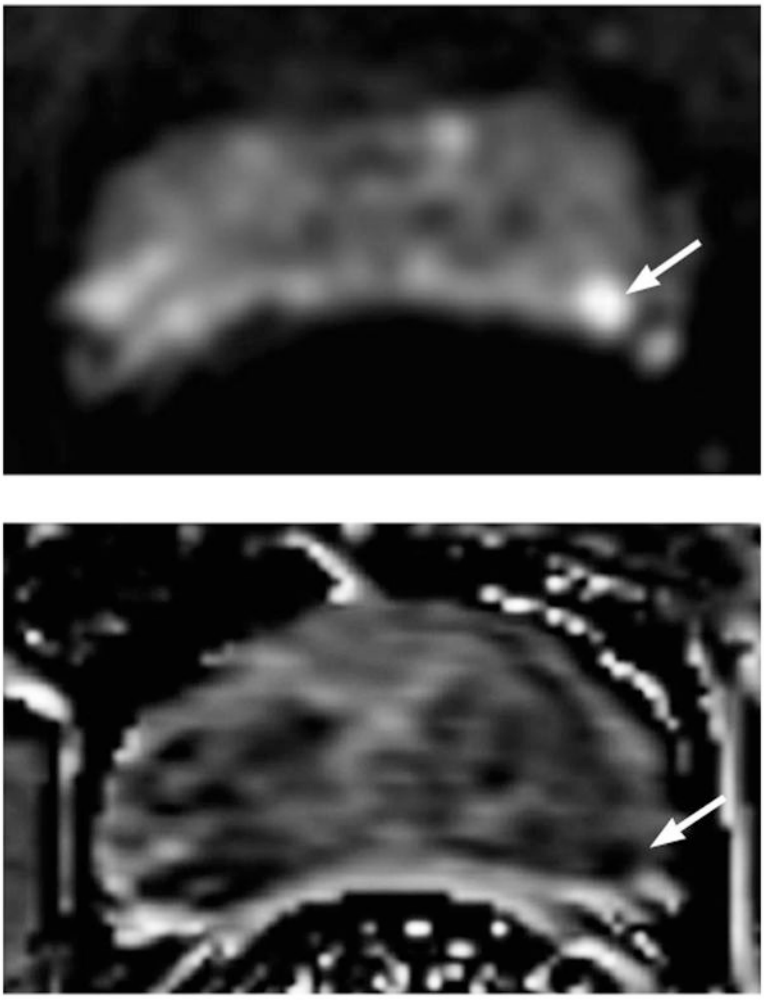

Figure 1.

Example prostate MR images from a 67-year-old (G3+3, PSA=4.6 ng/ml) untreated male (top panel: A-D) and from a 57-year-old man (G3+3, PSA=0.42 ng/ml) treated with 5α-reductase inhibitors (bottom panel: E-H). T2w intensity images (A, E), ADC (B, F), high-b value DWI intensity (C, G), and washout slope (D, H) images are shown. The arrows designate cancerous lesions.

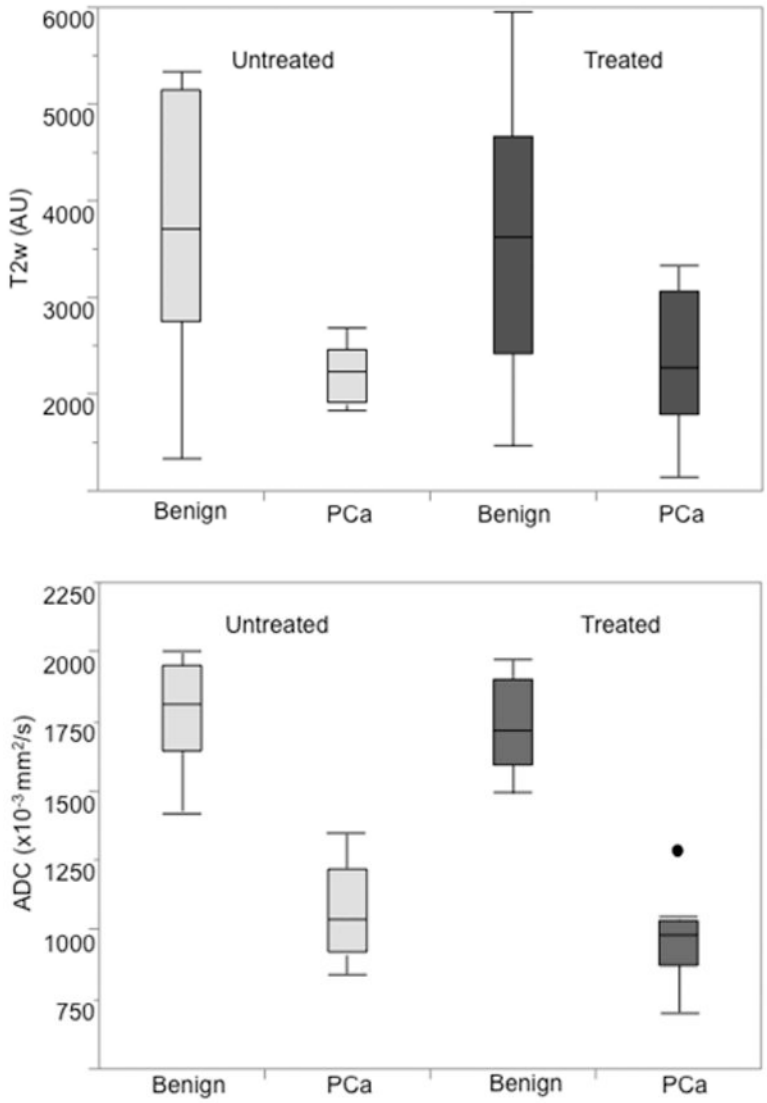

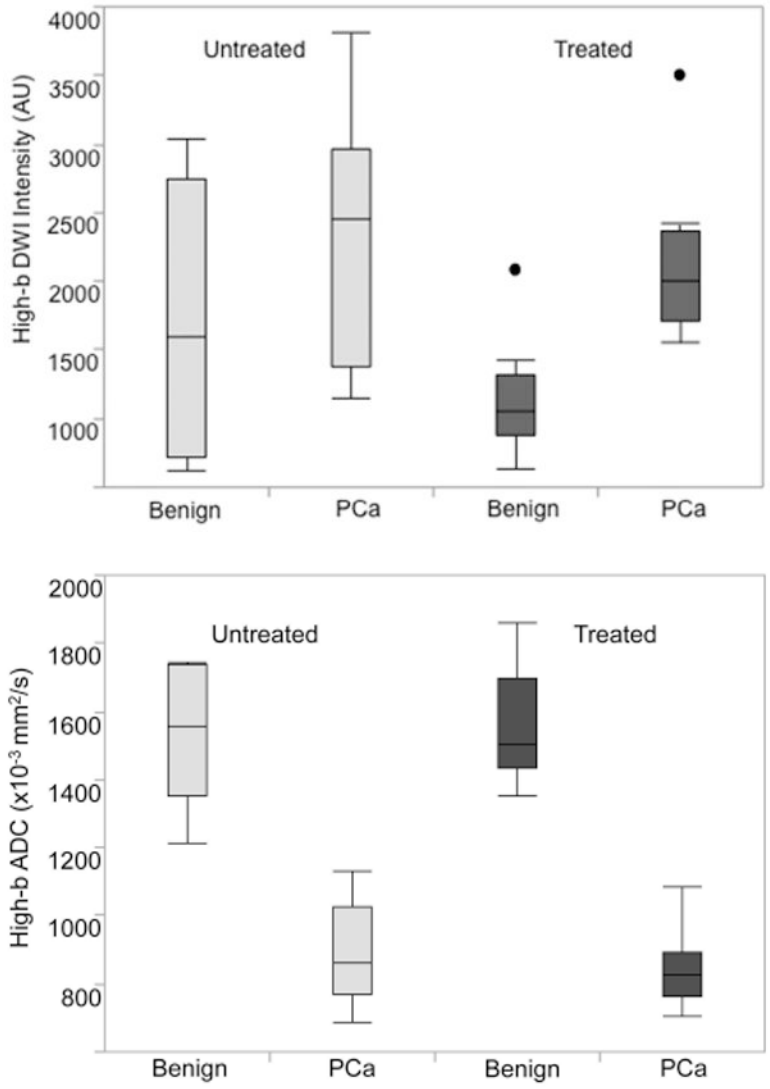

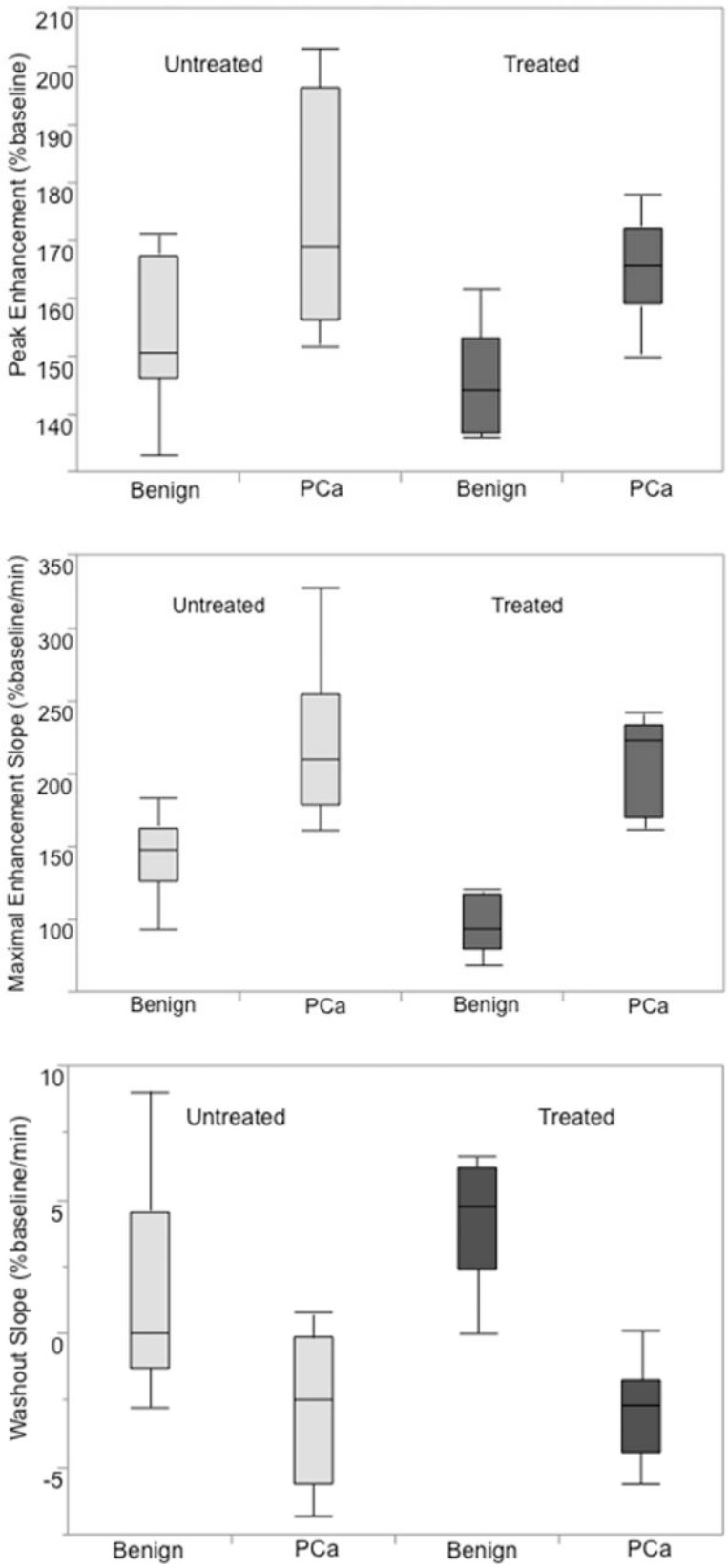

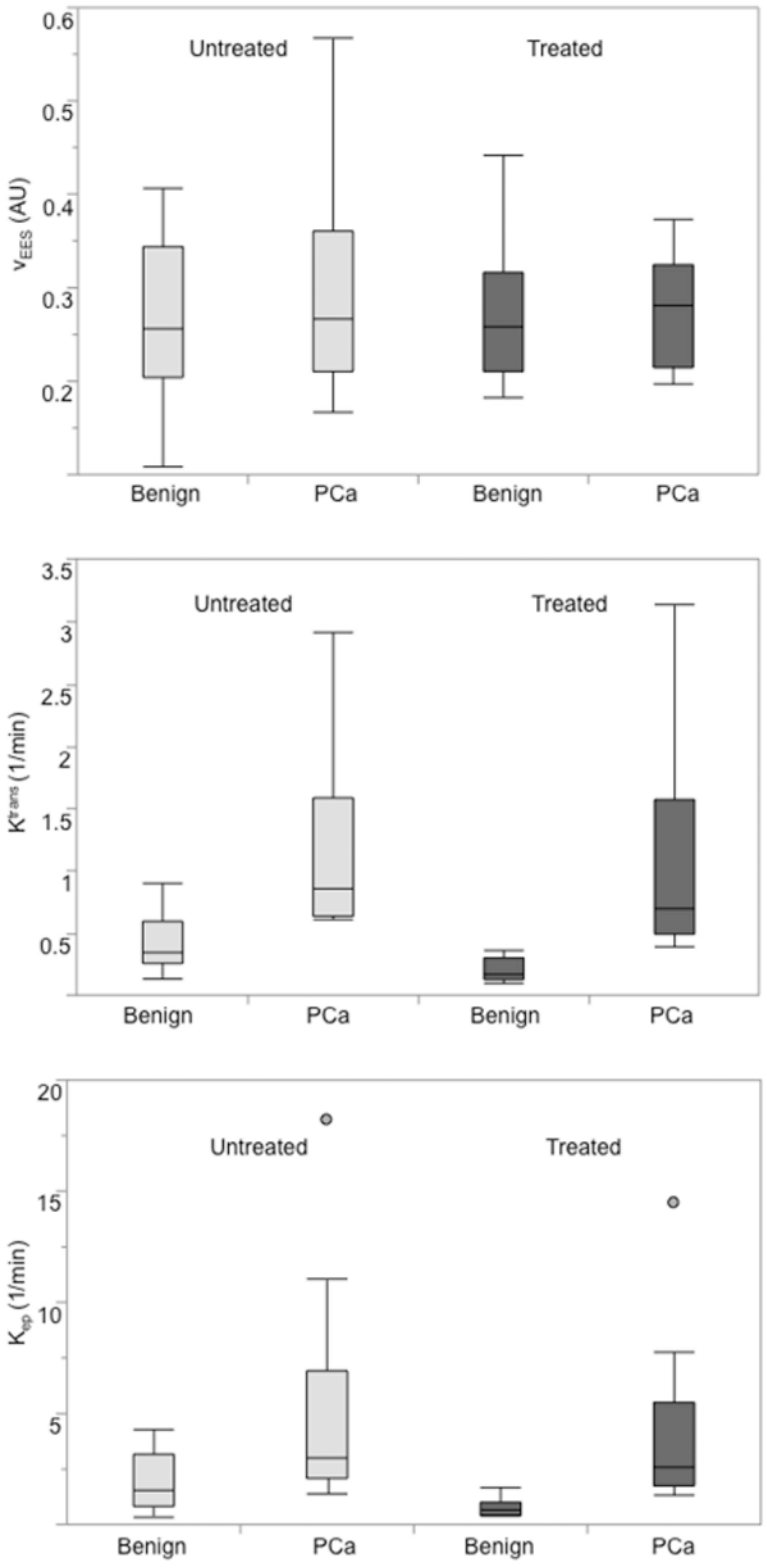

Figure 2.

Box-plots comparing A) T2w intensity, B) ADC (b=600 s/mm^2), C) high-b value DWI intensity, D) high-b ADC (b=1350 s/mm^2), E) peak enhancement, F) maximal enhancement slope, G) washout slope, H) v_{EES}, I) K^{trans}, and J) K_{ep} values in cancerous and benign prostatic tissues for untreated individuals and those treated with 5α-reductase inhibitors. Horizontal lines within the box plots represent the median values. Whiskers are drawn to the furthest points within 1.5× interquartile range, where interquartile range is the difference between the 1st and the 3rd quartiles.

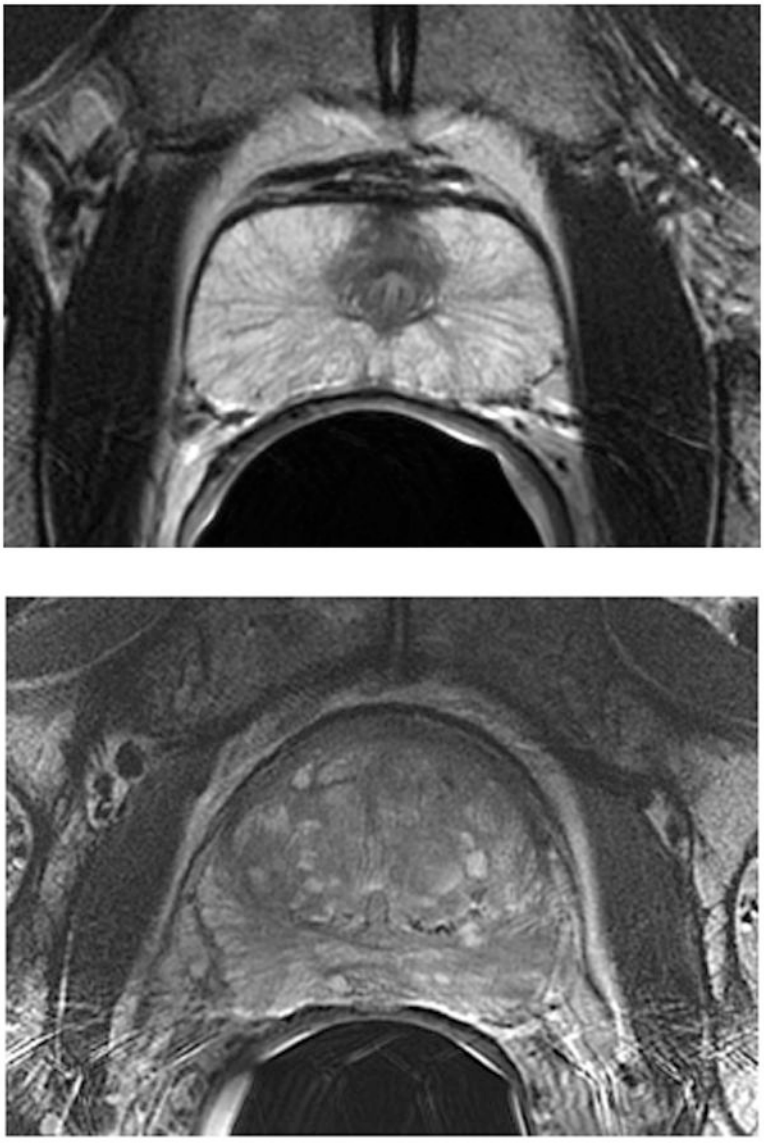

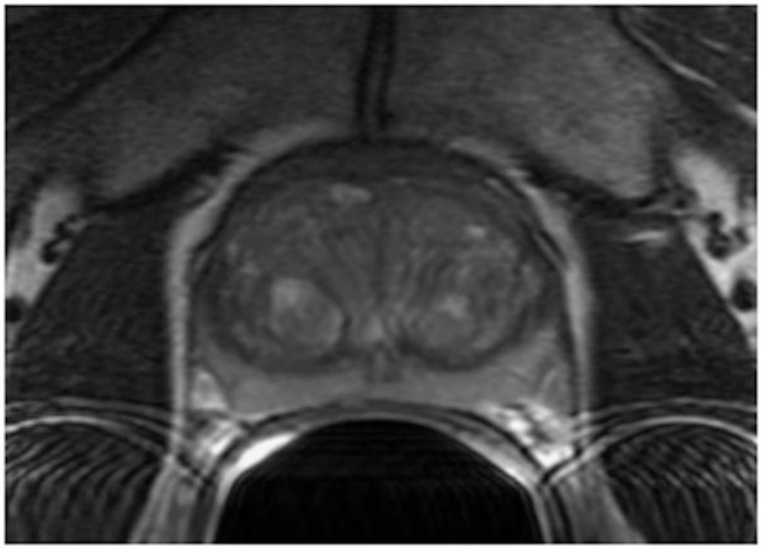

Figure 3.

T2-weighted images of benign prostatic tissues for A) untreated patient with homogeneous tissue (age = 64.1 years, PSA= 2.14 ng/ml, Gleason 3+3), B) untreated patient with heterogeneous tissue (71.4 years, 5 ng/ml, G3+3), C) 5-ARI treated patient with homogeneous tissue (50.4 years, 4.44 ng/ml, G3+3).

Table 1

Imaging parameters

Imaging	Pulse Sequence	TR/TE (ms)	FOV (cm)	Matrix Size	NEX	ST (mm)	In-Plane Res. (mm)	Temp. Res. (s)	b-value (s/mm^2)
T2w	FSE	6000/100	18×18	512×512	1	3	0.35×0.35	N/A	N/A
DCE	3D SPGR	3.5/0.9	26×26	256×256	0	3	1.02×1.02	10.417	N/A
Conv ADC	ss-EPI	4000/90	24×24	128×128	4	3	0.94×0.94	N/A	0, 600
rFOV ADC	ss-EPI	4000/90	18×9	128×64	6	3	0.70×0.70	N/A	0, 600
High-b DWI	ss-EPI	4000/100	24×24	256×256	5	3	0.94×0.94	N/A	0, 1350

FSE=Fast Spin Echo, SPGR = Spoiled Gradient Echo, ss-EPI = Single-Shot Echo-Planar Imaging, ST = Slice Thickness

Table 2

Patient Characteristics

Metric	Untreated			Treated		
	Mean±SD	**Median (Q1, Q3)**	**Minimum, Maximum**	**Mean±SD**	**Median (Q1, Q3)**	**Minimum, Maximum**
Prostate Volume (matched) [cc]	48.66±29.6	41 (29.9, 51.1)	24.3, 123.3	47.03±28.77	41.5 (29.5, 49.1)	18.8, 115
Age [years]	64.4±6.6	72.0 (65.6, 76.6)	53.6, 76.4	70.8±9.1	65.3 (60.0, 68.1)	57.4, 82.8
PSA (within 6 months) [ng/ml]	6.55±3.76	5.93 (4.20, 8.05)	1, 14.1	5.84±6.56	3.44 (1.90, 6.91)	1.2, 22.6
# Previous Biopsy Procedures	2.1±0.99	2 (1, 3)	1, 4	2.1±0.88	2 (1, 3)	1, 3
# Biopsy Cores obtained during the most recent biopsy	15.3±3.0	15 (12, 18)	12, 21	15.3±2.1	16 (13.5, 17)	12, 18
Days between the most recent biopsy and mpMRI	455±326	476 (166, 556)	68, 1093	1140±1364	624 (351, 988)	220, 4604
Size of benign ROIs [cm^2]	0.87±0.55	0.72 (0.54, 0.94)	0.33, 1.89	0.62±0.33	0.56 (0.37, 0.65)	0.31, 0.91
Size of cancerous ROIs [cm^2]	0.40±0.33	0.28 (0.20, 0.40)	0.11, 0.99	0.32±0.26	0.26 (0.13, 0.46)	0.03, 0.84

PSA=Prostate Specific Antigen, ROI = Region of Interest, SD = Standard Deviation.

Table 3

ROC-AUC for cancerous versus benign tissues in untreated and 5-ARI treated patients. The higher AUC values are listed in **BOLD**.

Imaging	Untreated ROC-AUC	Treated ROC-AUC
T2-weighted	0.82	**0.79**
ADC (b=600 s/mm^2)	1	**1**
High-b ADC (b=1350 s/mm^2)	1	**1**
High-b DWI	0.71	**0.94**
Maximal Enhancement Slope	0.95	**1**
Washout Slope	0.78	**0.99**
Peak Enhancement	0.84	**0.93**
Ktrans	0.9	**1**
Kep	0.8	**0.98**
vEES	0.51	**0.57**
Combined	0.86	**0.99**

The combined model used T2-weighted, ADC, maximal enhancement slope, washout slope, peak enhancement, K^{trans}, and K_{ep} for the untreated group and ADC, high-b DWI, maximal enhancement slope, washout slope, peak enhancement, K^{trans}, and K_{ep} for the treated group.

Table 4

Absolute coefficient of variation of the measures within cancer and benign tissues for the treated and untreated groups. The lower COV values are listed in **BOLD**.

Imaging	Benign		Cancer	
	Untreated	Treated	Untreated	Treated
T2-weighted	**0.34**	0.389	**0.233**	0.303
ADC (b=600 s/mm^2)	0.107	**0.095**	**0.153**	0.174
High-b ADC (b=1350 s/mm^2)	0.13	**0.103**	0.16	**0.13**
High-b DWI	0.567	**0.361**	0.367	**0.264**
Maximal Enhancement Slope	**0.185**	0.204	0.24	**0.153**
Washout Slope	2.556	**0.572**	0.968	**0.611**
Peak Enhancement	0.082	**0.064**	0.113	**0.052**
K^{trans}	0.556	**0.451**	**0.749**	0.83
K_{ep}	0.674	**0.52**	1.05	**0.965**
v_{EES}	0.353	**0.289**	0.394	**0.212**